Anharmonicity in lattice dynamics of Ce at the γ-α phase transition

Xupeng Yuan(袁旭鹏)[1], Hongxing Song(宋宏星)[1], Yi Sun(孙毅)[1], Fengchao Wu(吴凤超)[1], Hao Wang(王豪)[1,†], Yusong Huang(黄誉松)[1], Mohan Chen(陈默涵)[2], and Hua Y. Geng(耿华运)[1,2,*]

[1] *National Key Laboratory of Shock Wave and Detonation Physics, Institute of Fluid Physics, China Academy of Engineering Physics, Mianyang, Sichuan 621900, P.R. China;*
[2] *HEDPS, Center for Applied Physics and Technology, College of Engineering and School of Physics, Peking University, Beijing 100871, P.R. China.*

The nature of the γ and α phases in Ce, and the intriguing isostructural γ-α phase transition, are challenging and highly debated topics in condensed matter physics, which are usually attributed to the strong correlation of localized 4f electrons. On the other hand, lattice dynamics might also play an important role in this issue. However, there have been few studies devoted to exploring the effects of lattice dynamics in Ce, particularly the possible role of anharmonicity. In this work, a thorough and systematic investigation of anharmonicity in the lattice dynamics of Ce near the γ-α isostructural transition is carried out using the *ab initio* self-consistent phonon method. The required potential energy surface (PES) is obtained using DFT with the exchange-correlation (XC) functional selected by assessing various functionals. By taking the experimental isothermal equation of state (EOS) as the benchmark, we validate that the semi-local PBEsol functional is accurate enough to model the γ phase when the fully localized 4f electrons are placed in the core; on the other hand, the PBE functional with the 4f electrons in the valence space provides good agreement with the experimental data for the α phase. This practical approximation has the advantage of avoiding the explicit treatment of the strong correlations of localized 4f states, and leads to much higher computational efficiency if only forces are considered. The lattice dynamics and anharmonicity in the γ and α phases of cerium are investigated using the temperature-dependent effective potential (TDEP) and full temperature-dependent potential (FTDP) methods. Both methods reveal significant contributions from anharmonicity, especially the quantum sampling in FTDP, which brings the theoretical data into good agreement with the experimental data. Our results demonstrate that anharmonicity plays an important role in the lattice dynamics of cerium. These insights might be crucial for understanding the compression behavior of Ce and for developing efficient and accurate interatomic potentials for similar systems for large-scale molecular dynamics simulations.

Keywords: Anharmonicity, Equation of State, Lattice Dynamics, Isostructural Phase Transition.

PACS: 63.20.Ry, 71.15.Mb, 64.70.Kb

† To whom correspondence should be addressed. E-mail: wh_95@qq.com
* To whom correspondence should be addressed. E-mail: s102genghy@caep.cn

1. Introduction

Cerium (Ce), the first lanthanide element with one 4f electron, exhibits intriguing electronic characteristics with the 4f electron being intermediate between itinerant and localized states [1]. This dual nature leads to a variety of quantum phenomena, including antiferromagnetic ordering [2], superconductivity [3], and a series of pressure-induced structural phase transitions. Among them, the most striking might be the isostructural transition from γ-Ce to α-Ce observed under a pressure of 0.8 GPa at room temperature, or under ambient pressure at temperatures below 183 K [4]-[6]. This transition is accompanied by a large volume collapse of 14–17%, from the low-density ferromagnetic γ-Ce to the high-density paramagnetic α-Ce [7][9]. Extensive experimental and theoretical investigations have been carried out to understand the correlation with 4f electron behavior. Nonetheless, the exact role of 4f electrons in this transition remains debated.

Currently, the Mott transition (MT) mechanism [1][10] and Kondo volume collapse (KVC) mechanism [11][12] have been proposed to describe the evolution of 4f electrons during this phase transition. The MT assumes that the 4f electron is itinerant in the α phase but becomes localized in the γ phase. On the other hand, the KVC model emphasizes the hybridization between the localized 4f electron and the conduction electrons, which means that the 4f electron is localized in both α and γ phases of Ce, whereas the two phases exhibit fundamental differences in their Kondo temperature. It was estimated that the Kondo temperature in γ-Ce is approximately 50-100 K, while in α-Ce it is significantly higher, reaching 1000-2000 K [13]. It should be noted that both models neglect the lattice degrees of freedom and thus do not include the entropy contributions from lattice vibrations [14]. On the other hand, the importance of phonon contributions to the γ-α transition at finite temperature should not be underestimated [15][16].

Experimentally, the lattice dynamics of the α and γ phases has been investigated using inelastic neutron scattering (INS) and inelastic X-ray scattering (IXS) techniques [4][8][9][17][21]. Based on experimental data, Amadon et al. [22] pointed out that during the phase transition, the variation in the vibrational entropy contribution is significantly greater than that of internal energy, particularly near the critical temperature, where the entropy contribution becomes even more pronounced. Current first-principles studies on the lattice dynamics of cerium are predominantly based on the harmonic approximation (HA) [14][15][21][23][24], and have revealed significant changes in phonon dispersion during the γ-α transition. This observation suggests that lattice degrees of freedom should be considered to properly describe the phase transition.

It should be emphasized that in α-Ce, significant deviations between theoretical and experimental phonon spectra were observed in the TA [110] and TA [111]

branches [15][21][23]. These deviations may originate from the strong correlation effects of 4f orbitals, or from the neglect of anharmonicity in the phonons calculated with the HA method. In γ-Ce, the pronounced phonon frequency softening near the L point was attributed to the strong correlations of 4f electrons, and was modeled by using HA with DFT+U and in ferromagnetic ordering [15]. All other conventional DFT calculations (also in HA) overestimate the phonon energies relative to the experimental data [21]. Notably, the energy of DFT+U is not well defined and depends on its U and J parameters. Therefore, all theoretical calculations reported so far cannot reproduce the phonon dispersions of both α and γ phases accurately. For example, for γ-Ce, the maximum deviation between theoretical and experimental data for the LA modes can reach as large as 11.91% at the X point and 12.15% at the L point [21], while for TA modes it reaches 16.83% [21] at the X point and 67.50% [23] at the L point. Despite this substantial discrepancy, there is little consideration of advanced lattice dynamics methods beyond HA, and several studies just simply attributed this discrepancy to the contributions of strong correlation effects of 4f electrons. Some even artificially scaled down the calculated phonon spectra by a factor for the purpose of matching the experimental data [21]. Such a discrepancy stands as a challenging issue for understanding the behavior of Ce.

On the other hand, first-principles calculations such as density functional theory (DFT) [25][26] have been applied to study the γ and α phases of cerium, as well as the transition between them, for decades. Early DFT calculations usually employed the local density approximation (LDA) or generalized gradient approximation (GGA), which were unable to describe the γ phase of Ce (with the lattice parameter underestimated by 12% in LDA and by 8% in GGA) when the 4f electrons were placed in the valence space [27][30]. It should also be noted that these calculations were unable to reproduce the double-well solution in the E-V curve, even when electronic and vibrational entropy contributions were included [15][31][32]. It was later realized that, due to the strong electronic state change in the localized 4f state, it is practically unattainable for a single state-of-the-art DFT functional to describe both phases simultaneously [33][34]. Although some hybrid functionals can reproduce the double-well structure successfully [35], the predicted bulk modulus for the α phase remains overestimated.

Actually, current DFT is still incomplete and suffers from accuracy problems when correlations become strong. For example, most local and semi-local XC functionals are unable to fully capture the localization behavior of electrons quantitatively [36][38]. On the other hand, advanced hybrid functionals or model Hamiltonians, such as DFT+U or DFT+DMFT (dynamical mean-field theory), which show good promise for strongly correlated systems, lack the adaptive flexibility when the electronic state becomes delocalized. Their accuracy might deteriorate as the electronic correlations decrease. They even suffer from unexpected orbital localization errors in some transition metals, such as vanadium and niobium [39]. It is generally accepted that each functional is only an approximation to the exact XC functional within a narrow range. For the γ and α phases of cerium, which exhibit significant changes in electronic correlation, it is appropriate to use different but

suitable functionals for each phase, rather than a single functional for all phases. With this strategy, several investigations have shown that combining local-spin-density (LSD) and self-interaction-corrected LSD (SIC-LSD) can produce a satisfactory estimate for the equation of state (EOS) of the two phases [32][40][41]. Other methods that are specifically designed for strongly correlated systems have also been applied to cerium. By combining the LDA and LDA+U methods [42][43], Wang et al. [15] reconstructed the phase diagram of Ce, incorporating entropy contributions. Other examples include hybrid functionals [16][35][44] and the combination of LDA and DMFT (LDA+DMFT) methods [45][47]. Nonetheless, the computational demands of these methods such as SIC, hybrid functionals, and LDA+DMFT are high, rendering them impractical for first-principles molecular dynamics simulations. Besides solving the above-mentioned lattice dynamics issue, the rapidly developing machine learning potentials and large-scale molecular dynamics simulations also require accurate and efficient evaluation of energies and forces from DFT calculations. This underscores the importance of finding an effective and efficient semi-local XC functional that can produce energies and forces with competitive accuracy for Ce.

To this end, in this work the performance of a wide range of available functionals for the α and γ phases of Ce is systematically explored, with primary focus on the balance between accuracy and computational demand. The aim is not to identify a universal XC functional, but to reveal which XC functional is more suitable for the respective regimes of the two phases of Ce. It should be emphasized that this work does not propose using different XC functionals for different phases in phase diagram calculations (even though this might be possible if the respective energies of all phases are carefully realigned). Future work should pursue a single theoretical framework that can consistently describe both phases to ensure a common energy reference. The remainder of this paper is organized as follows: The methods and computational details are presented in Sec. II. Section III presents the results, as well as the detailed discussions. The main findings are then summarized in Sec. IV.

2. Method and Computational Details

In order to find the suitable effective semi-local XC functional for the α and γ phases of Ce, we employ the experimental isothermal EOS as the benchmark. The XC functional whose P-V curve is closest to the experimental curve is selected for subsequent calculations. Except for the highly computationally demanding DFT+DMFT, a wide range of available XC functional categories is explored to ensure that the XC functionals are evaluated as comprehensively as possible. This includes the commonly used LDA and GGA (along with variants such as PBE, PW91, and PBEsol), and other advanced types of XC functionals: (i) hybrid functionals, such as PBE0 [48] and HSE06 [49], admix a fraction of Hartree-Fock exact exchange into the density functional; (ii) DFT+U and DFT+J [39] incorporate effective Hubbard models to describe localized or delocalized states; (iii) meta-GGA and SCAN functionals [50], which include the Laplacian of the electron density. For the hybrid functional and DFT+U calculations of the γ phase, we also consider the option of placing the localized 4f electrons in the valence space. The calculated P-V data points are fitted to

a third-order Birch-Murnaghan EOS model [51], and the resulting fit is then systematically compared with available experimental data.

For the PBE+U calculations, the effective Hubbard parameters are selected as follows: for the γ phase, U_{eff} = 1.6 eV (U = 1.6 eV and J = 0 eV) [15]; for the α phase, we tested U_{eff} = 5.4 eV (U = 6.1 eV and J = 0.7 eV) [42], 2.0 eV (U = 2.0 eV and J = 0 eV), and 1.6 eV (U = 1.6 eV and J = 0 eV). The PBE+J method, whose formalism is similar to DFT+U [39], is a semi-empirical Hubbard model to address the localization error in DFT. We calculate a series of J values between 0.5 eV and 6 eV with a step of 0.5 eV. For the EOS calculations, an fcc primitive cell with one Ce atom is employed. The DFT calculations are performed using the Vienna Ab initio Simulation Package (VASP) [52], and the projector augmented-wave (PAW) [53] method is used. We take the 4f electrons in α-Ce as partially itinerant, and the $4f^{1}5s^{2}5p^{6}6s^{2}5d^{1}$ configuration is placed in the valence space. For γ-Ce, except for the hybrid functional and DFT+U calculations, we take the 4f electrons as fully localized and put them into the core, thus the valence electron configuration is $5s^{2}5p^{6}6s^{2}5d^{1}$. The electronic SCF convergence threshold is set to 1×10^{-6}eV and the kinetic energy cutoff for the plane-wave basis is 550 eV. The k-point mesh size for this setting is 20×20×20.

The harmonic phonon dispersion is calculated using the frozen phonon and small-displacement methods [54][55]. To calculate the anharmonic phonons, we use the TDEP [56][57] and FTDP [58] methods. For the former, a series of classical *ab initio* molecular dynamics (AIMD) simulations is carried out to sample the classical distribution on the potential energy surface (PES) [56][57]. For the latter, a series of *ab initio* path integral molecular dynamics (AI-PIMD) [59] simulations is carried out to sample the full temperature-dependent PES of the true quantum distribution [58]. For both methods, the forces are provided by first-principles DFT calculations with the given XC functional via the Hellmann-Feynman theorem. The displacements and the corresponding forces on each atom extracted from the AIMD and AI-PIMD simulations are then employed to determine the force constants and the dynamical matrices of the system, which then give the corresponding phonon spectra for the two simulations [58].

For lattice dynamics calculations, we use a 5×5×5 supercell that contains 125 atoms, with the Brillouin zone sampling performed using an 8×8×8 Monkhorst-Pack k-point mesh [60]. The AIMD and AI-PIMD simulations are carried out in the NVT ensemble at a temperature of 300 K. The time step is 1 fs, and each simulation lasts for 10000 steps. The AIMD simulations are carried out using VASP code, and AI-PIMD simulations are performed with our home-made MyPIMD code [61]. For both the α and γ phases, 80 independent configurations are extracted from the AIMD/AI-PIMD trajectories. Static DFT calculations with a 2×2×2 Monkhorst-Pack k-point mesh are then carried out to generate sufficiently accurate Hellmann-Feynman atomic forces for these configurations. We then use MyPHON, which is based on the PHON program [62], to obtain both the harmonic and anharmonic phonon dispersions

for α and γ-Ce at the finite-temperature of T=300 K.

3. Results and Discussion

3.1. Effective XC functional performance and EOS

For first-principles methods based on DFT, a reliable XC functional that can achieve a good balance between accuracy and computational efficiency is critical for investigating the vibrational properties, phase transition mechanisms, as well as large-scale MD simulations. Our exploration covers a wide range of commonly available XC functionals and their combinations. Within them only hybrid functionals and LDA+DMFT methods can produce a double-well structure on the E-V curve for the γ and α phases of Ce. However, even for these promising functionals, they cannot describe the properties in terms of lattice constant and bulk modulus of both α and γ phases satisfactorily at the same time, in spite of the fact that the γ-α transition can be predicted by the same functional qualitatively (see Supplementary Material). This observation further underscores the argument that currently most state-of-the-art XC functionals are only effective approximations and cover (and thus are applicable to) only a small range of the whole spectrum of the exact DFT. With this insight, it becomes evident that the most practical strategy for applying current DFT to a complex system is to combine different approximate XC functionals for different phases or compression regions. In particular, for the isothermal P-V curve, there is no single functional available so far that can reproduce the experimental data measured at 300 K exactly. The theoretical P-V curves of the α and γ phases as calculated with different XC functionals are shown in Figs. 1 and 2, respectively. For clarity of presentation, here only representative results are displayed. Other results are compiled in the Supplementary Material (SM).

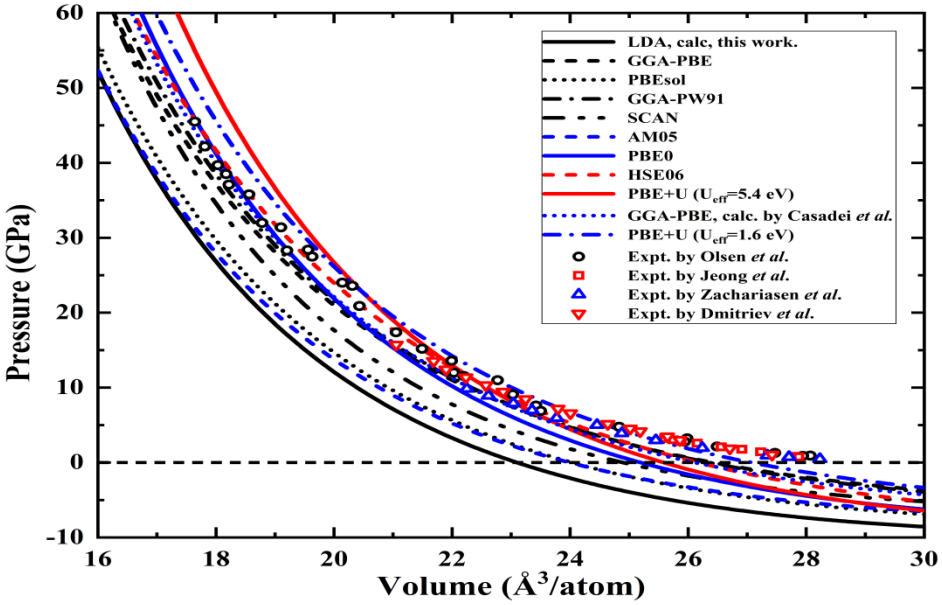


Fig. 1. (Color online) Comparison of the calculated isothermal P-V curves of α-Ce at

0 K using different XC functionals with the 300 K experimental data [8][63][65].

Notably, for α-Ce, the LDA, PBEsol, AM05, and SCAN functionals significantly overestimate the density at a given pressure across the explored pressure range. The deviation can be as large as 21.49%. PBE+U with U_{eff}=5.4 eV also shows poor performance, with a deviation in density of 2.97% at 0 GPa. For a smaller value of U (e.g., U_{eff}=1.6 eV), PBE+U gives a better lattice constant at 0 GPa, but there is not much improvement on the slope of the P-V curve. Furthermore, the predicted P-V curve deviates significantly from the experimental one when the pressure is above 5 GPa. Hybrid functionals give a deviation as large as 11.39% in density at 0 GPa. In contrast, the GGA-PW91 and GGA-PBE functionals have similar overestimation in density at low pressure with a deviation at a level of 6.51% and 6.23%. Their performance improves with increasing pressure. We note that when spin-orbit coupling (SOC) is included, the small deviation in the PBE functional calculations at low pressure still persists, indicating that SOC has negligible influence on α-Ce and therefore can be practically neglected.

For γ-Ce (see Fig. 2), it is evident that the LDA functional overestimates the density by 3.89% at 0 GPa; whereas at 0.7 GPa, the deviation reduces to 0.87%. For PBEsol, the deviation in the density from the experimental data is 0.43% at 0 GPa, and is 3.15% at 0.7 GPa. For comparison, the advanced SCAN, hybrid HSE06, and PBE+U functionals have deviations in density as large as 6.29% at 0 GPa and 8.46% at 0.7 GPa. Note that by fine-tuning the value of U_{eff}, we find that PBE+U with U_{eff}=1.6 eV can match the experimental data near 0 GPa. However, it deviates from the physical expectations at high density, with an unphysical maximum in the P-V curve at about 19 Å^3/atom.

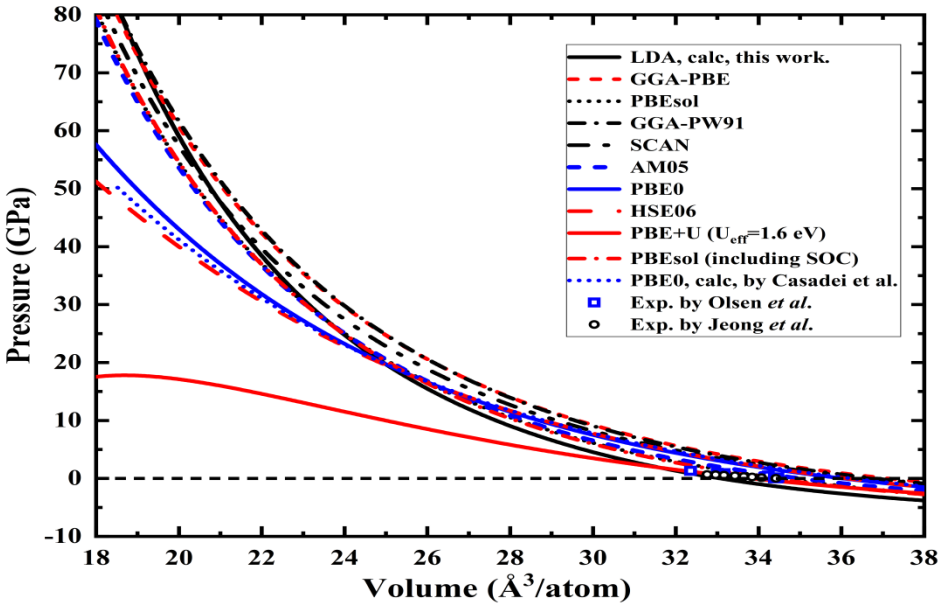


Fig. 2. (Color online) Comparison of the calculated isothermal P-V curves of γ-Ce at 0 K using different XC functionals with the 300 K experimental data [8][63].

Based on the above analysis, we adopt PBEsol for γ-Ce and PBE for α-Ce in the following anharmonicity calculations. To further assess the performance of the selected functionals, the equilibrium atomic volume, bulk modulus, and its pressure derivative are summarized in Table I. The calculated bulk modulus for α-Ce with the PBE functional is 39.1 GPa and for γ-Ce with the PBEsol functional is 33.0 GPa, showing deviations of 34.8% and 57.1%, respectively. Nevertheless, the calculated bulk modulus of α-Ce is higher than that of γ-Ce, indicating that the compressibility of α-Ce is lower, consistent with the experiment. It should be noted that the calculations for the α and γ phases employ different XC functionals and pseudopotentials. Therefore, their total energies do not share a common energy reference. Consequently, we do not attempt to compute the γ-α transition pressure directly. Our analysis focuses on EOS parameters (bulk modulus, compressibility) for each phase separately, which are insensitive to the energy reference.

Table I. Calculated equilibrium atomic volume V_0 ($Å^3$), bulk modulus B_0 (GPa) and its pressure derivative B_0' for α- and γ-Ce at 0 K compared with the experimental data at zero pressure and 300 K.

		This work	Experiments
α-Ce (PBE)	V_0	26.42	29.0 [63], 28.06 [66]
	B_0	39.11	29 [63], 27 [8]
	B_0'	4.67	5.5 [63], 5.0 [67]
γ-Ce (PBEsol)	V_0	34.52	34.37 [66], 34.48 [63]
	B_0	33.00	21.0 [63]
	B_0'	4.03	—

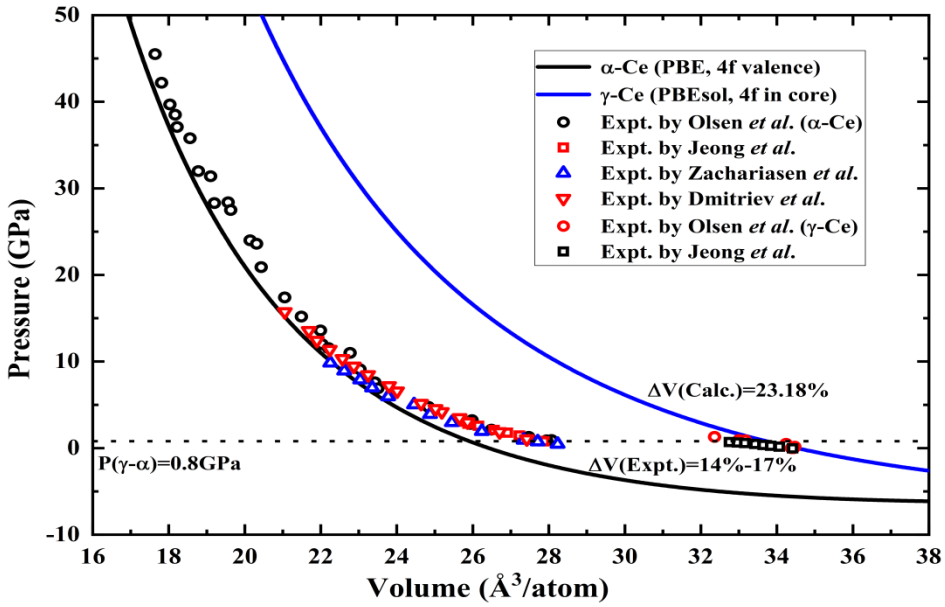


Fig. 3. (Color online) Comparison of theoretical and experimental P-V curves for α-Ce and γ-Ce.

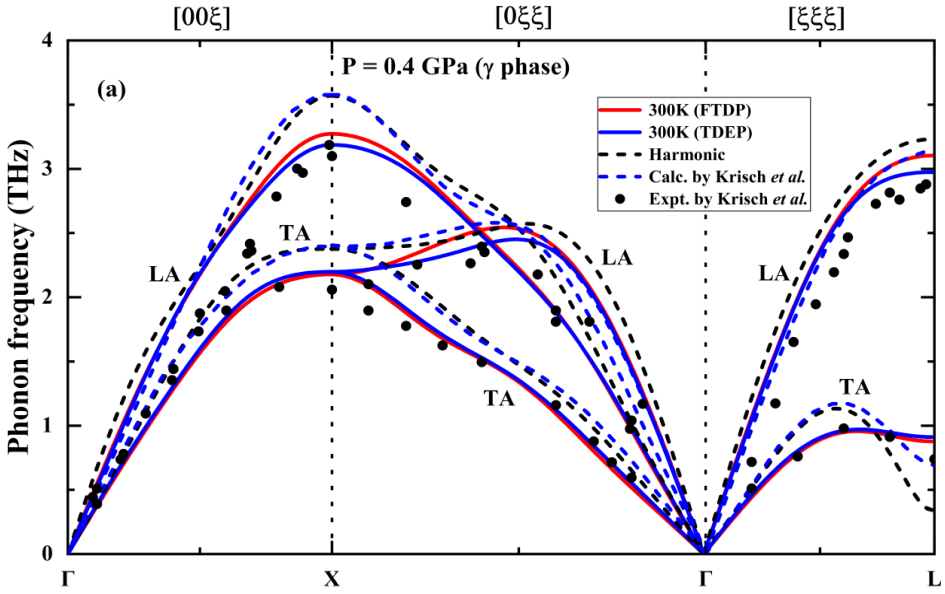
The calculated P-V curves for α-Ce and γ-Ce are compared with experimental data in Fig. 3. Using these curves at the experimental transition pressure of 0.8 GPa, we obtain V_γ=33.73 Å^3/atom and V_α=25.91 Å^3/atom, yielding a volume collapse of 23.18%, which overestimates the experimental value of 14-17%. This overestimation is consistent with the known tendency of semi-local functionals to underestimate the electronic correlation strength of the 4f electrons in Ce. Although this value shows a quantitative deviation, it successfully captures the essential feature of a significant volume discontinuity near the transition pressure. While the calculated compressibility also deviates from the experiment (Fig. 3), this does not undermine subsequent analysis. For the purposes of this study, anharmonicity in lattice dynamics is governed by higher-order derivatives of the potential energy surface, not by its curvature (bulk modulus). The chosen functionals are adequate for investigating anharmonicity in Ce.

3.2. Lattice dynamics and anharmonicity

For the γ-Ce at 0.4 GPa and 0.6 GPa, phonon calculations are performed at the experimental lattice constants of a = 5.120 Å (0.4 GPa) and 5.105 Å (0.6 GPa) that were measured at T = 300 K [21]. All calculations show no imaginary frequencies, indicating the dynamical stability at 0 K. Our harmonic phonon dispersion (HA) for γ-Ce at these pressures is in good agreement with previous theoretical results [21]:

the frequencies are significantly higher than the experimental values. In Ref. [21], it was suggested that this was due to the strong correlation effects that cannot be captured by DFT, and an overall scaling of the phonon frequencies by a factor of 0.9 was proposed to match the experimental data.

We further compute the lattice dynamics using more accurate methods that include anharmonicity, at both the classical level of TDEP and the quantum level of FTDP. The results are shown in Fig. 4, which are quite unexpected. They are both in good agreement with the experimental data, in sharp contrast to the HA, suggesting that the artificial scaling in Ref. [21] is unnecessary and the previously reported deviation might not be due to strong electronic correlation but to the HA in phonon calculations. In particular, at 0.6 GPa, the deviation at the X point decreases from 11.38% with the HA to 2.77% (for TDEP) and 2.15% (for FTDP) for the LA modes, and decreases from 16.83% with the HA to 4.95% (for TDEP) and 2.97% (for FTDP) for the TA modes. The improvement at the L point is more drastic: the large deviation with the HA (about 10.81% for the LA mode and 67.50% for the TA mode) is reduced to 6.76% (for the LA mode) and 13.75% (for the TA mode) when the FTDP method is employed, whereas the TDEP with classical AIMD sampling gives a 2.03% deviation for the LA mode at the L point. We also note that the HA fails to capture the bending in the TA[111] branch and the shape of the TA[110] branch qualitatively, whereas both branches are successfully reproduced when anharmonicity is included. The same improvement by anharmonicity is also observed at 0.4 GPa. This demonstrates that the lattice dynamics of γ-Ce can be accurately described by a semi-local XC functional and anharmonicity, if the 4f electrons are treated in the core. It is consistent with the established picture that 4f electrons remain fully localized in γ-Ce, but gradually become itinerant in α-Ce. These findings underscore the critical importance of anharmonicity in lattice vibrations for an accurate description of the γ phase of Ce.



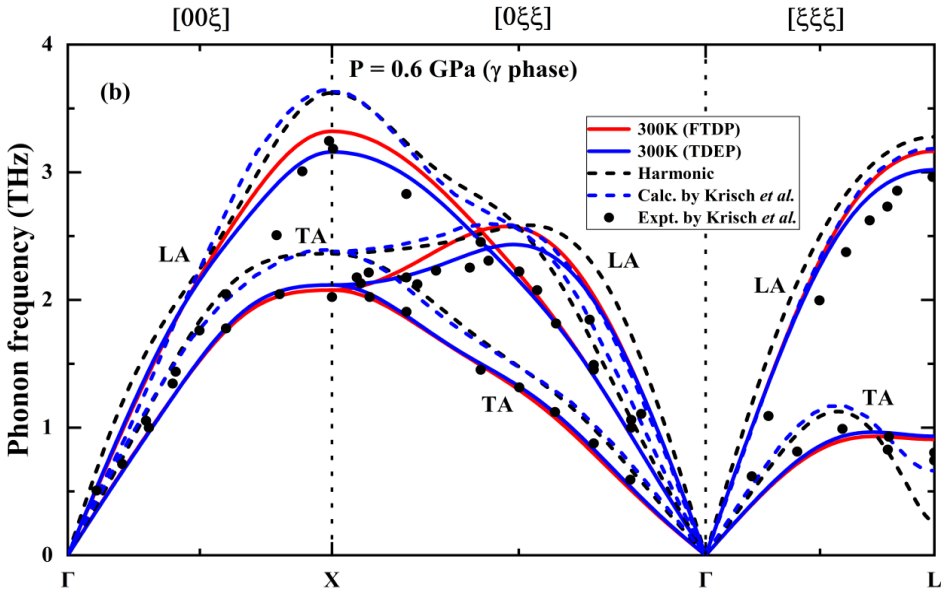


Fig. 4. (Color online) Comparison of harmonic (dashed lines) and anharmonic (red and blue solid lines correspond to the FTDP and TDEP results, respectively) phonon dispersions of γ-Ce at 0.4 GPa (a) and 0.6 GPa (b) with IXS experimental data at 300 K (black dots), as well as other theoretical harmonic results by Krisch et al. [21].

The phonon dispersion results for α-Ce at 0.8 GPa and 2.5 GPa are shown in Fig. 5. The calculations are carried out at the experimental lattice constants of 4.799 Å (0.8 GPa) and 4.687 Å (2.5 GPa) that were measured at T = 300 K [21], respectively. Similar to γ-Ce, there are no imaginary frequencies, demonstrating that this phase is dynamically stable. For all HA results, significant deviations are observed away from the experimental data along the Γ-L [ξξξ] and Γ-X [0ξξ] directions. In particular, at 0.8 GPa, the deviation in the LA mode is about 8.73% at the X point, and 8.51% at the L point. The largest deviation reaches about 57.14% and 35.63% in the TA mode at the L point for P = 0.8 and 2.5 GPa, respectively. This large discrepancy was previously attributed to the strong correlation of the 4f electrons. However, it could also come from anharmonicity that has not been investigated so far. The effects of anharmonicity cause a shift in phonon frequencies and can therefore significantly affect the thermodynamic properties of the material [68]. To examine this possibility, we compare the experimental data with anharmonic phonons calculated with TDEP and FTDP. As can be seen from Fig. 5, the theoretical phonon dispersion is greatly improved after including anharmonicity. Especially, the largest deviation at the X point is reduced to 6.63%, and the deviation at the high-symmetry point L is reduced from 57.14% to 51.95% at 0.8 GPa with FTDP. It should also be noted that TDEP has a relatively large error compared with the fully quantum FTDP, with the deviation of the former being 59.74% at the L point, whereas it reduces to 51.95% for the latter.

We also noticed that when the pressure increases from 0.8 GPa to 2.5 GPa, the frequencies of both TDEP and FTDP for the LA branch at both the X and L points increase.

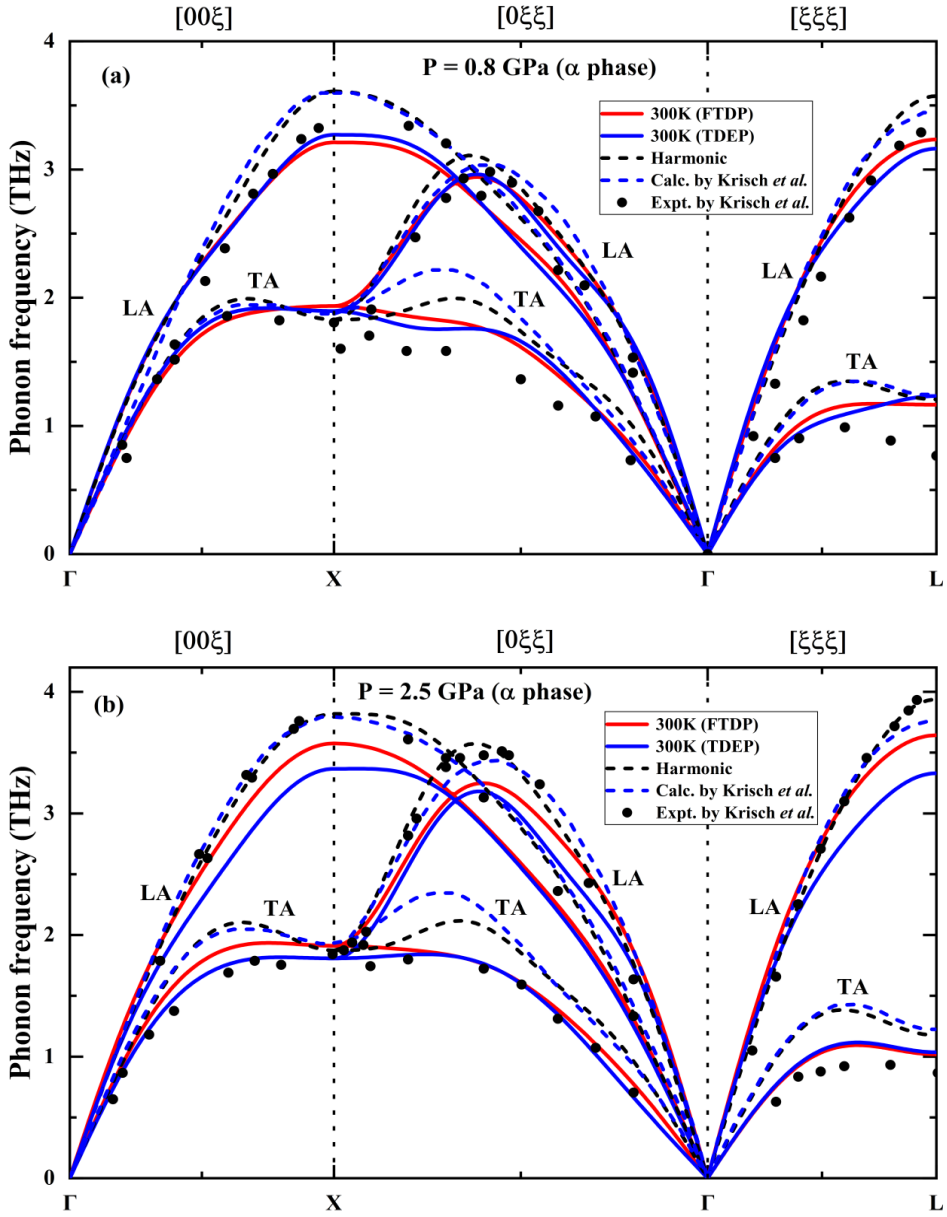


Fig. 5. (Color online) Comparison of our calculated harmonic (dashed lines) and anharmonic (red and blue solid lines correspond to the FTDP and TDEP calculation results, respectively) phonon dispersions of α-Ce at 0.8 GPa (a) and 2.5 GPa (b) with IXS experimental data at 300 K (black dots), as well as other theoretical harmonic results by Krisch et al. [21].

At 2.5 GPa, both TDEP and FTDP show larger deviations from the experimental data than the HA, particularly at higher frequencies. This behavior may be attributed to the mismatch in error cancellation and the residual strong correlations of the 4f electrons. We noticed that for other branches anharmonicity gives overall better phonon spectra than the HA, indicating that both methods might involve error

cancellation. For the HA, the error cancellation comes from strong correlation effects and anharmonicity, whereas for the TDEP and FTDP methods, it mainly comes from the intrinsic inaccuracies of the XC functionals employed in standard DFT calculations. The apparent improvement of the HA over TDEP and FTDP at this pressure may be attributed to both a fortuitous cancellation of errors in the HA and the residual strong correlations of 4f electrons in α-Ce.

To further investigate this discrepancy, both experimental and theoretical uncertainties should be considered. On the experimental side, the IXS data could be affected by pressure calibration, sample quality, and non-hydrostatic conditions. As noted in Ref. [21], the crystal quality degraded slightly in α-Ce, which could introduce additional uncertainty in the high-pressure measurements. On the theoretical side, the remaining deviations may arise from the treatment of anharmonicity and the XC functional. Therefore, future IXS measurements under hydrostatic conditions, combined with in-situ X-ray diffraction to verify phase purity and systematic calculations using different functionals and anharmonic methods, would help distinguish experimental uncertainties from theoretical limitations and provide a more reliable benchmark for the lattice dynamics of Ce near the γ-α transition.

The mode Grüneisen parameters $\gamma_q=-\partial \ln\omega_q/\partial \ln V$ across the γ-α transition (γ-Ce at 0.6 GPa and α-Ce at 0.8 GPa) derived from TDEP phonon dispersions are shown in Fig. 6. Positive values correspond to an increase in phonon frequency with pressure, while negative values may indicate the precursor of a phase transition or the presence of electron-phonon coupling. Our results reveal that γ_q ranges from -0.60 to 2.79, exhibiting a pronounced wave-vector dependence. The most prominent negative region appears around the X point, where the γ_q values of the TA modes drop to -0.60, consistent with the experimental observations of negative mode γ_q [21], and indicating substantial changes in electron-phonon coupling in this region. Furthermore, one TA branch attains a maximum of 2.79 near the Γ point; The LA mode also reaches a maximum of approximately 1.36 at the same wave vector. The marked difference in γ_q between the TA and LA modes indicates that the responses of different vibrational modes to the volume collapse are fundamentally distinct. These findings provide evidence that lattice dynamics plays a critical role in the γ-α transition of Ce.

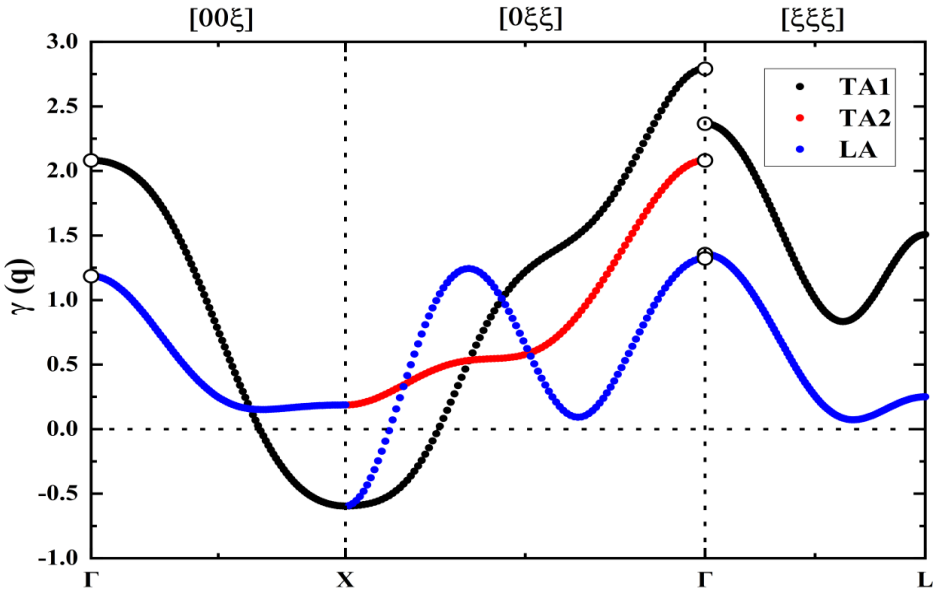


Fig. 6. (Color online) Mode Grüneisen parameters across the γ-α transition in Ce derived from TDEP phonon dispersions.

The Debye temperatures (Θ_D) of γ-Ce (0.4 and 0.6 GPa) and α-Ce (0.8 and 2.5 GPa) calculated using the HA, TDEP, and FTDP methods are summarized in Table II, together with the experimental results. All three methods reproduce the key behavior of Θ_D, which increases with pressure and exhibits a discontinuity at the γ-α phase transition. Among them, the HA systematically overestimates Θ_D at all pressures. In contrast, the TDEP method yields results that agree well with the experimental values, overestimating Θ_D by 3.25% for γ-Ce at 0.6 GPa and by 1.30% for α-Ce at 0.8 GPa, while for α-Ce at 2.5 GPa it underestimates Θ_D by 7.32%. The remaining discrepancy in the TDEP results may partly arise from the limitations in the description of electron-phonon coupling. The FTDP method yields Θ_D between the HA and TDEP values.

Table II. Debye temperatures (in K) calculated from HA, TDEP, and FTDP methods for γ-Ce and α-Ce.

P (GPa)	a_0 (Å)	HA	TDEP	FTDP	Experiment [21]
0.4 (γ)	5.120	138.2	129.1	131.1	122
0.6 (γ)	5.105	138.9	127.0	130.5	123
0.8 (α)	4.799	149.2	139.8	140.5	138

2.5 (α)	4.687	164.7	145.5	151.1	157

Furthermore, from the TDEP results of Θ_D near the phase boundary (127.0 K for γ-Ce at 0.6 GPa and 139.8 K for α-Ce at 0.8 GPa), the vibrational entropy change is estimated as $|\Delta S_{vib}^{\gamma-\alpha}|=3k_B\ln\left(\frac{139.8}{127.0}\right)=0.29k_B$. This value is in good agreement with the ultrasonic measurement of $0.32k_B$ on polycrystalline samples [69] and in reasonable agreement with the inelastic X-ray scattering result of $0.33\pm0.03k_B$ by Krisch et al. [21], but is about a factor of 2.5 lower than that derived by Jeong et al. from their neutron and X-ray diffraction work [8]. Despite this discrepancy, our results indicate that the lattice vibrational contribution to the γ-α phase transition is not negligible.

With this understanding of the prominent anharmonicity in the γ and α phases of cerium, we are now in a position to reassess previous interatomic potentials which did not consider anharmonicity when they were constructed. For example, Sheng et al. [70] fitted the EAM potential to the experimental phonons using the harmonic approximation, which might misrepresent the anharmonic effects in the experimental data and lead to an inaccurate potential. We examine this by calculating the anharmonic phonons of the γ and α phases of Ce by using this EAM potential with both the TDEP and FTDP methods. The results (Fig. S4 in SM) indicate that this potential can reproduce the experimental phonon spectra (0.6 GPa for γ-Ce and 0.8 GPa for α-Ce) when anharmonicity is included, although some deviations can still be observed. Especially, the TA mode along the Γ-L direction for γ-Ce and the TA mode along the Γ-X and Γ-L directions for α-Ce are greatly improved by anharmonicity. However, the agreement with the experimental data deteriorates for the LA mode along the Γ-L direction for γ-Ce, as well as for the right branch of the TA mode along the X-Γ direction for α-Ce. This illustrates that this potential has good error cancellation between anharmonicity and interatomic interaction. Nonetheless, this balance of error cancellation might fail if large atomic displacements are involved (see Fig. S5 in SM). Using this re-assessed EAM potential and the associated anharmonic phonon free energy, we further compute the thermal pressure contributed by lattice dynamics within a range from ambient pressure up to 8 GPa for the α and γ phases. The correction to the P-V curve is then given by $P(V, T) = P_c(V) + P_{vib}(V, T)$. At T = 300 K, the final P-V curve for the γ and α phases is plotted as dashed lines in Fig. 7. It can be seen that the thermal pressure effect is very

small for both α-Ce and γ-Ce.

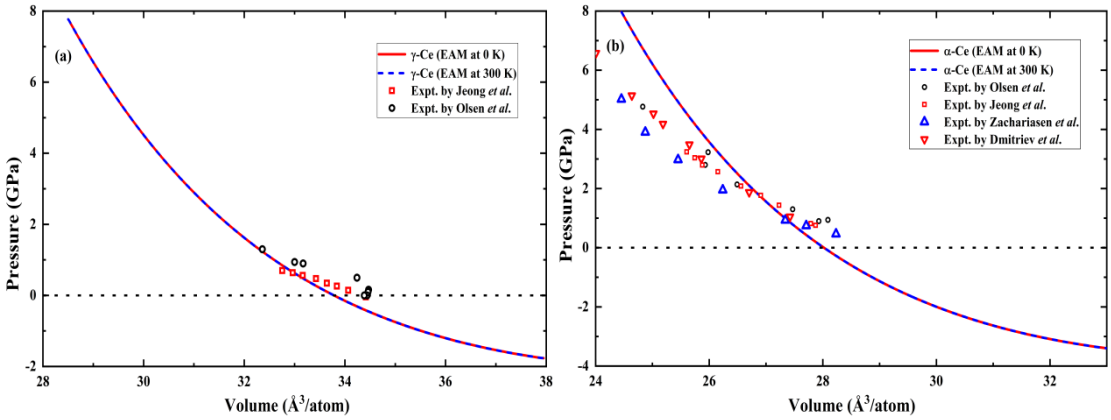


Fig. 7. (Color online) Comparison of the calculated isothermal P-V curves of γ-Ce (a) and α-Ce (b) using the EAM potential including thermal contribution with experimental data at 300 K [8][63][65].

The results presented above demonstrate that the PBE and PBEsol functionals, combined with the TDEP and FTDP methods, provide a satisfactory description of the lattice dynamics of Ce across the γ-α transition. To examine whether a functional that performs better for the EOS would necessarily yield improved phonon dispersions, we also assessed the recently developed LAK meta-GGA functional [71]. Although it reasonably reproduces the experimental P-V curve of Ce, as well as the double-well shape, its phonon dispersions deviate considerably from the experimental data. This indicates that the apparently good performance of LAK on the γ-α transition is due to subtle but fragile error cancellation. This balance is easily disrupted when atoms move away from their ideal positions. This is confirmed by AIMD simulations where the LAK functional suffers from difficulties in achieving electronic self-consistency in DFT calculations (see SM for details).

4. Conclusions

This study systematically investigated the important role of anharmonicity in lattice dynamics of Ce at the γ-α isostructural phase transition. Taking the experimental isothermal EOS as the benchmark, we showed that the semi-local PBEsol functional is accurate enough to model the γ phase when the fully localized 4f electrons are placed in the core; on the other hand, the PBE functional with the 4f electrons in the valence space provides good agreement with the experimental data for the α phase. In this way, it might be possible to avoid the explicit treatment of strongly correlated 4f electrons when only ionic motions are considered, thus significantly enhancing computational efficiency. The lattice dynamics and

anharmonicity in the α and γ phases of cerium were investigated using TDEP and FTDP methods, which reduce the maximal phonon spectrum deviations from 67.50% (γ-Ce, TA mode at the L point) and 57.14% (α-Ce, TA mode at the L point) of the harmonic approximation to 13.75% and 51.95%, respectively, while reproducing key features such as the TA[111] branch bending well. This finding challenges the traditional perception about the impact of the strong correlations of 4f electrons on the lattice dynamics. This work indicates that anharmonicity plays an important role in the lattice dynamics of cerium and may provide a practical framework for high-throughput and large-scale molecular dynamics simulations of this strongly correlated metal.

Acknowledgement

This work was supported by the National Key R&D Program of China under Grant No. 2021YFB3802300, the Foundation of National Key Laboratory of Shock Wave and Detonation Physics (No. 2023JCJQLB05401), and the National Natural Science Foundation of China under Grant Nos. 12404287, 12372370, 12274381. Part of the simulation was performed on resources provided by the center for Comput. Mater. Sci. (CCMS) at Tohoku University, Japan.

References

[1] Johansson B, Abrikosov I A, Alden M, Ruban A V and Skriver H L 1995 *Phys. Rev. Lett.* **74** 2335
[2] Lock J M 1957 *Proc. Phys. Soc. Sect. B* **70** 566
[3] Wittig J 1968 *Phys. Rev. Lett.* **21** 1250
[4] Lipp M J, Jackson D, Cynn H, Aracne C, Evans W J and McMahan A K 2008 *Phys. Rev. Lett*. **101** 165703
[5] Munro K A, Daisenberger D, MacLeod S G, McGuire S, Loa I, Popescu C, Botella P, Errandonea D and McMahon M I 2020 *J. Phys.: Condens. Matter* **32** 335401
[6] Wu Y, Fang Y, Li P, Xiao Z H, Zheng H, Yuan H Q, Cao C, Yang Y F and Liu Y 2021 *Nat. Commun.* **12** 2520
[7] Devaux N, Casula M, Decremps F and Sorella S 2015 *Phys. Rev. B* **91** 081101
[8] Jeong I K, Darling T W, Graf M J, Proffen T, Heffner R H, Lee Y, Vogt T and Jorgensen J D 2004 *Phys. Rev. Lett.* **92** 105702
[9] Decremps F, Antonangeli D, Amadon B and Schmerber G 2009 *Phys. Rev. B* **80** 132103
[10] Johansson B 1974 *Phil. Mag.* **30** 469
[11] Allen J W and Martin R M 1982 *Phys. Rev. Lett*. **49** 1106
[12] Allen J W and Liu L Z 1992 *Phys. Rev. B* **46** 5047
[13] Lavagna M, Lacroix C and Cyrot M 1982 *Phys. Lett. A* **90** 210
[14] Huang L and Chen C A 2007 *J. Phys.: Condens. Matter* **19** 476206

[15] Wang Y, Hector L G, Zhang H, Shang S L, Chen L Q and Liu Z K 2008 *Phys. Rev. B* **78** 104113
[16] Casadei M, Ren X, Rinke P, Rubio A and Scheffler M 2016 *Phys. Rev. B* **93** 075153
[17] Stassis C, Gould T, McMasters O D, Gschneidner Jr K A and Nicklow R M 1979 *Phys. Rev. B* **19** 5746
[18] Stassis C, Loong C K, McMasters O D and Nicklow R M 1982 *Phys. Rev. B* **25** 6485
[19] Manley M E, McQueeney R J, Fultz B, Swan-Wood T, Delaire O, Goremychkin E A, Cooley J C, Hults W L, Lashley J C, Osborn R and Smith J L 2003 *Phys. Rev. B* **67** 014103
[20] Antonangeli D, Farber D L, Aracne C M, Ruddle D G, Siebert J and Bonner B P 2010 *High Press. Res*. **30** 151
[21] Krisch M, Farber D L, Xu R and Johansson B 2011 *Proc. Natl. Acad. Sci. U.S.A*. **108** 9342
[22] Amadon B, Biermann S, Georges A and Aryasetiawan F 2006 *Phys. Rev. Lett*. **96** 066402
[23] Hu C E, Zeng Z Y, Zhang L, Chen X R and Cai L C 2011 *Physica B* **406** 669
[24] Cadien A, Hu Q Y, Meng Y, Cheng Y Q, Chen M W, Shu J F, Mao H K and Sheng H W 2013 *Phys. Rev. Lett*. **110** 125503
[25] Hohenberg P and Kohn W 1964 *Phys. Rev.* **136** B864
[26] Kohn W and Sham L J 1965 *Phys. Rev.* **140** A1133
[27] Min B I, Jansen H J F, Oguchi T and Freeman A J 1986 *Phys. Rev. B* **34** 369
[28] Eriksson O, Brooks M S S and Johansson B 1990 *Phys. Rev. B* **41** 7311
[29] Söderlind P, Eriksson O, Johansson B and Wills J M 1994 *Phys. Rev. B* **50** 7291
[30] Jarlborg T, Moroni E G and Grimvall G 1997 *Phys. Rev. B* **55** 1288
[31] Wang Y 2000 *Phys. Rev. B* **61** R11863
[32] Lüders M, Ernst A, Däne M, Szotek Z, Svane A, Ködderitzsch D, Hergert W, Györffy B L and Temmerman W M 2005 *Phys. Rev. B* **71** 205109
[33] Perdew J P and Zunger A 1981 *Phys. Rev. B* **23** 5048
[34] Kümmel S and Kronik L 2008 *Rev. Mod. Phys.* **80** 3
[35] Liu Y, Ren X, Geng H Y and Chen M H 2022 *New J. Phys*. **24** 093032
[36] Geng H Y, Chen Y, Kaneta Y and Kinoshita M 2007 *Phys. Rev. B* **75** 054111
[37] Geng H Y, Chen Y, Kaneta Y, Iwasawa M, Ohnuma T and Kinoshita M 2008 *Phys. Rev. B* **77** 104120
[38] Geng H Y, Song H X, Jin K, Xiang S K and Wu Q 2011 *Phys. Rev. B* **84** 174115
[39] Wang Y X, Geng H Y, Wu Q and Chen X R 2020 *J. Chem. Phys*. **152** 024118
[40] Szotek Z, Temmerman W M and Winter H 1994 *Phys. Rev. Lett*. **72** 1244
[41] Svane A 1994 *Phys. Rev. Lett*. **72** 1248
[42] Amadon B, Jollet F and Torrent M 2008 *Phys. Rev. B* **77** 155104
[43] Shick A B, Pickett W E and Liechtenstein A I 2001 *J. Electron Spectrosc. Relat. Phenom*. **114** 753
[44] Casadei M, Ren X, Rinke P, Rubio A and Scheffler M 2012 *Phys. Rev. Lett*. **109** 146402

[45] Held K, McMahan A K and Scalettar R T 2001 *Phys. Rev. Lett*. **87** 276404
[46] Chen Q Y, Feng W, Xie D H, Lai X C, Zhu X G and Huang L 2018 *Phys. Rev. B* **97** 155155
[47] Kim J, Ryu D C, Kang C J, Kim K, Choi H, Nam T S and Min B I 2019 *Phys. Rev. B* **100** 195138
[48] Perdew J P, Ernzerhof M and Burke K 1996 *J. Chem. Phys.* **105** 9982
[49] Krukau A V, Vydrov O A, Izmaylov A F and Scuseria G E 2006 *J. Chem. Phys*. **125** 224106
[50] Sun J, Ruzsinszky A and Perdew J P 2015 *Phys. Rev. Lett*. **115** 036402
[51] Birch F 1978 *J. Geophys. Res*. **83** 1257
[52] Kresse G and Furthmüller J 1996 *Comput. Mater. Sci*. **6** 15
[53] Blöchl P E 1994 *Phys. Rev. B* **50** 17953
[54] Parlinski K 2007 *J. Phys.: Conf. Se*r. **92** 012009
[55] Parlinski K, Li Z Q and Kawazoe Y 1997 *Phys. Rev. Lett*. **78** 4063
[56] Hellman O, Abrikosov I A and Simak S I 2011 *Phys. Rev. B* **84** 180301
[57] Hellman O, Steneteg P, Abrikosov I A and Simak S I 2013 *Phys. Rev. B* **87** 104111
[58] Geng H Y 2022 *J. Phys. Chem. C* **126** 19355
[59] Chandler D and Wolynes P G 1981 *J. Chem. Phys*. **74** 4078
[60] Monkhorst H J and Pack J D 1976 *Phys. Rev. B* **13** 5188
[61] Geng H Y 2015 *J. Comput. Phys.* **283** 299
[62] Alfè D 2009 *Comput. Phys. Commun*. **180** 2622
[63] Olsen J S, Gerward L, Benedict U and Itié J P 1985 *Phys. B+C* **133** 129
[64] Ellinger F H and Zachariasen W H 1974 *Phys. Rev. Lett*. **32** 773
[65] Dmitriev V P, Kuznetsov A Y, Bandilet O, Bouvier P, Dubrovinsky L, Machon D and Weber H P 2004 *Phys. Rev. B* **70** 014104
[66] Koskenmaki D C and Gschneidner Jr K A 1978 *Handbook on the Physics and Chemistry of Rare Earths* (Amsterdam: North-Holland) p. 337
[67] Olsen J S, Gerward L, Dancausse J P and Gering E 1993 *Phys. B* **190** 92
[68] Zhang T X, Zhou K, Li Y J, Yi C H, Faizan M, Fu Y H, Wang X J and Zhang L J 2025 *Chin. Phys. B* **34** 046301
[69] Voronov F F, Vereshchagin L F and Goncharova V A 1961 *Sov. Phys. Dokl.* **5** 1280
[70] Sheng H W, Kramer M J, Cadien A, Fujita T and Chen M W 2011 *Phys. Rev. B* **83** 134118
[71] Giri A, Shahi C and Ruzsinszky A 2025 *Phys. Rev. B* **112** 125115